ELSEVIER

S0032-3861(96)00677-5

Polymer Vol. 37 No. 25, pp. 5577–5582, 1996

0032-3861/96/$15.00+0.00

Characterization of latex blend films by atomic force microscopy

Abhijit A. Patel, Jianrong Feng, Mitchell A. Winnik*, G. Julius Vancso‡
Department of Chemistry, University of Toronto, Toronto, Ontario, Canada M5S 1A1

and Carla B. Dittman McBain
ICI Paints, North America Strongsville Research Center, 16651 Sprague Rd, Strongsville, OH 44136, USA
(Received 6 November 1994; revised 15 February 1995)

Analysis of latex blend films, made possible by TappingMode™ atomic force microscopy, has provided insight into the interaction properties of hard and soft latex particles. Looked at in isolation, the hard latex forms a cracked and opaque film with no detectable particle deformation, while the soft latex coalesces into a transparent coating showing small domains with face-centred-cubic arrays. In blends where the soft component is present in amounts greater than 40% by volume, smoothed bumps are observed which appear larger than either the hard or soft particles alone. The smoothness of each bump, supported by other evidence, suggests that the soft particles have coalesced into a virtual continuum at the surface, while the overall surface unevenness is thought to be indicative of underlying hard particles. We interpret the submersion of the hard particles as arising because of the lower surface energy of the soft polymer.

(Keywords: latex films; emulsion polymers; water-borne coatings)

INTRODUCTION

One of the classic dilemmas in the field of water-borne coatings is how to achieve continuous and void-free polymer coatings with a glass transition temperature T_g above room temperature from an aqueous dispersion of polymer particles[1]. If the particles are sufficiently soft, they will deform and become space filling as the water evaporates. Unfortunately, because of the low T_g, the film produced will be tacky to the touch. If the dispersion is comprised of high T_g latex, the compliance is too small for the forces accompanying drying to deform the particles into a continuous film. The traditional solution to this problem has been to add volatile plasticizers to the dispersion[2,3]. These coalescing aids promote deformability by lowering the T_g of the latex, but evaporate from the film to leave a high T_g coating with good block resistance in place. While the solvents used in this way are not considered to be toxic, they do contribute to volatile organic emissions. The move toward environmentally friendly coatings requires that these contributors to VOC (volatile organic compounds) emissions be removed from the formulation. Thus new strategies for film formation are needed.

One possible strategy is the use of latex blends[4,5]. In such blends, one might expect that the soft particles deform and fill the voids between the hard particles, behaving somewhat like a glue, while the hard particles ought to provide block resistance and contribute to the strength and integrity of the film. Transparency should be achieved if the refractive indices of the two components are not too different and if the hard component is well dispersed in the final film. While this strategy is being actively investigated in industry, there are few publications in the open literature to describe the properties of these blends.

We are interested in understanding the conditions under which transparent films are formed from latex blends. Part of this process involves describing the morphology of these blends, both in bulk and at the surface. Here, using an atomic force microscope (a.f.m.) in the TappingMode™, we examine the surface structure of a series of latex blends prepared from mixtures of a high T_g latex dispersion and a low T_g latex dispersion. AFM is a very useful technique for studying the surface of latex films[6]. To simplify the problem, we choose a pair of particles similar in chemical composition and nearly identical in size. Both are poly(methylmethacrylate-*co*-butylacrylate) [P(MMA-BA)] copolymers. The hard particles of diameter $d = 111$ nm and $T_g = 48°C$ contain less BA than the soft particles of $d = 103$ nm and $T_g = 17°C$. The refractive indices of the two polymers are very similar, estimated to be 1.486 and 1.483, respectively.

EXPERIMENTAL

Materials and film preparation

Butylacrylate (BA), methylmethacrylate (MMA), and a proprietary surface active monomer were used as received. Ammonium persulfate and the polyoxyethylene alkyl ether phosphate surfactant Lubrophos LK500 (Rhône Poulenc) were also used as received. All batches utilized monomers that contained a small amount of

* To whom correspondence should be addressed
‡ Present address: University of Twente, Faculty of Chemical Technology, PO Box 217, NL-7500 AE Enschede, The Netherlands

inhibitor added by the manufacturer to prevent polymerization from occurring during shipping.

Polymerizations using persulfate as initiator were run at 75°C in a nitrogen-purged, agitated 5 litre Morton flask. Anionic stabilized latex was produced by creating a seed latex of approximately 38 nm diameter comprised of a BA : MMA weight ratio of 61 : 31. The seed polymerization is followed by a homogeneous 4.5 h feed with BA : MMA monomer ratios of 28 : 40 and 46 : 53 for the targeted 44°C T_g and the 10°C T_g latex polymers, respectively. The surface active monomer was 1 wt%, and the surfactant charge was 2 wt%, based upon polymer solids. Analogous non-ionic stabilized latexes were also prepared.

As measured by differential scanning calorimetry, the soft particles when dry have a T_g of 17°C and for the hard particles the T_g is 48°C. Particle sizes were measured using a disc centrifuge. Both samples had narrow size distributions with mean diameters of 103 nm (soft) and 111 nm (hard). In the experiment described here, both types of particles are stabilized by 2 wt% anionic surfactant based upon latex solids.

Blends were prepared by combining known amounts of each of the two dispersions at 48 wt% solids and mixing the samples thoroughly. In preparing the films for AFM, two methods of application were attempted. In the first method, a drop of diluted (12 wt%) dispersion was placed onto a freshly cleaved mica surface using a Pasteur pipette. The second approach was to use a fine artist's paintbrush to paint a concentrated latex dispersion (48 wt%) onto the mica surface. Films were allowed to dry at 22°C and ambient humidity (54%). The second method leads to flatter film surfaces which are easier to image.

Phase diagram

The films for the phase diagram (transparency *versus* blend composition) were prepared by a slightly different method and on a thin glass substrate. Two drops of a latex dispersion at 48 wt% solids (of various compositions) were placed onto a microscope coverslip using a Pasteur pipette. The liquid was then spread evenly over most of the area of the coverslip using a paintbrush. Again, the films were dried under ambient conditions overnight. The transparency measurements were taken by placing the coverslips individually in the sample beam of a Hewlett Packard 8452A diode array spectrometer and measuring the transmittance *versus* air in the range 400–700 nm. The percentage transmittance at an arbitrary wavelength of 550 nm was recorded and plotted *versus* composition on the phase diagram.

Atomic force microscope

The atomic force microscope used was a Nanoscope III from Digital Instruments Inc., Santa Barbara, CA. The microscope was placed on a vibration isolation puck, and images were taken under ambient conditions. The theoretical aspects of atomic force microscopy are detailed elsewhere[7,8]. The images were acquired exclusively in the TappingMode™ using a silicon tip. This operation mode allows imaging of delicate samples with essentially zero shear forces and with normal forces on the order of fractions of a nanoNewton. The tip was raster-scanned over the samples to produce an image of 512 × 512 pixels. The scan rate was kept below 2 Hz to ensure adequate tracking of surface features. All images were auto-flattened in the y-direction by a computer to correct for drift in piezo extension over the time of the scan.

RESULTS AND DISCUSSION

Phase diagram

The first feature of interest in the formation of latex blends is whether the films formed are transparent. In a recent study on films prepared from blends of latex particles with very different compositions, a plot of transmittance *versus* composition showed a sharp transition from opaque to clear at a volume fraction of soft particles approaching 50%[4,9]. Transparency depended on the drying rate of the samples. By freeze fracture electron microscopy (FFTEM) we could see that cloudiness or opaqueness of fully dense films was associated with aggregation of the hard particles in the film.

The phase diagram obtained as a plot of transmittance *versus* composition for the two P[MMA-BA] latex samples is shown in *Figure 1*. Here, where the index of refraction difference between the two latex polymers is smaller than in the example described above, hard-particle aggregation should cause much less light scattering. Turbidity should arise primarily from voids and cracks associated with the failure to form fully dense films. Examination of *Figure 1* suggests that there are two transitions in the phase diagram. At a volume fraction $\phi_s > 0.2$ of soft component, the films become light transmitting. There is a gradual transition as the fraction of soft component in the blend is increased, and full transparency (82%–85% T) is reached at $\phi_s = 0.5$. The transparency at $\phi_s > 0.5$ corresponds to that of a PMMA film on glass of comparable film thickness.

Visual observations were in accord with measurements of percentage transmittance. At soft particle volume fractions of 0.5, and greater, the films were clear and continuous. As the volume fraction of soft polymer was decreased below 0.5, cracks became progressively more pronounced, and the extent of cracking was closely

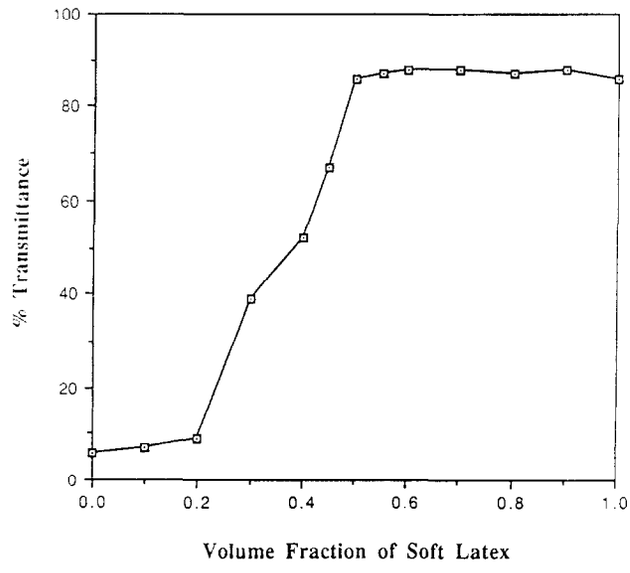

Figure 1 Phase diagram for film transparency: a plot of percentage transmittance at 550 nm *versus* ϕ_s

related to film turbidity. The severity of cracking ranged from a few large cracks in the $\phi_s = 0.45$ sample to many random as well as centrally radiating cracks in the $\phi_s = 0.2$ sample. Large cracks are normally an indication that drying occurs too quickly for the compliance of the polymer to accommodate (by flow) the contraction of the polymer which accompanies loss of water from the film. Microcracks and microvoids in the film, if they are extensive, will make a greater contribution to light scattering. Their presence is an indication of the inability of the soft polymer to fill completely the spaces between the individual hard particles.

AFM images

Examination by atomic force microscopy of the various films we prepared showed that the flatness and uniformity of the films was much better when the paintbrush was used. In the diluted drop method, the film thickness on the mica was found to be about 30 μm, while the painting method produced films with thicknesses of about 10 μm. We believe that the shear forces associated with the painting action contribute to the greater surface uniformity of the painted films.

To appreciate the changes in the latex blends, it is instructive to first look at the pure hard and pure soft films under AFM Several perspectives of the higher T_g latex are shown in *Figure 2*, and corresponding images of films of the lower T_g latex are shown in *Figure 3*. The 1 μm × 1 μm three-dimensional and height images provide a detailed view of the particle arrangement, whereas the 2.5 μm × 2.5 μm three-dimensional images are intended to illustrate the local uniformity of the film surface. The difference between the two particle types is dramatic. The hard particles remain undeformed and spherical, whereas the soft particles have coalesced into a virtually continuous film with small ordered regions.

The newly-innovated TappingMode™ is especially suited to accurate imaging of the soft surfaces which we encountered in our investigation. In normal contact mode AFM, the tip is in virtual contact with the surface of the sample, and experiences a constant downward force while being raster-scanned over a certain area. Although the force is usually very small, it often causes microscopic damage to the surface being scanned. In the TappingMode™, however, such scraping is eliminated. The mode of detection employs a tip which vibrates above the sample and whose oscillation amplitude is damped by lightly tapping the hydration layer on the sample. Because the surface is not significantly disturbed, the images obtained in this way provide a much more accurate description of soft surface topologies.

When the dispersions of hard particles dry, we obtain AFM images that show that the particles are distributed randomly over the surface of the film, with no ordering apparent when viewed from above[10]. The cross-section of the surface, visible in the 3D image, shows that the particles have remained spherical. The particle size seems to agree with the 111 nm value measured for the dispersion. The AFM cannot be relied upon for an absolute measurement of the particle size due to well-known tip imaging artefacts. One possibility to reduce the masking effect of the tip is to improve the image by deconvolution procedures, as suggested by Markiewicz and Goh[11].

The AFM images of the soft particles show excellent coalescence, but with the boundaries of the individial particles still visible at the surface. This is a special situation, observed here because the temperature of drying was just slightly higher than the glass transition temperature of 17°C. The particles deform, but polymer interdiffusion is not sufficient to make the interparticle boundaries disappear. Small spaces are sometimes observed at the junction of three or more particles. These holes result from the imperfect juxtaposition of ordered domains, and they may also serve as tiny channels which facilitate the evaporation of water during the last stages of drying. The particle size appears to be close to the 103 nm value found for the dispersion,

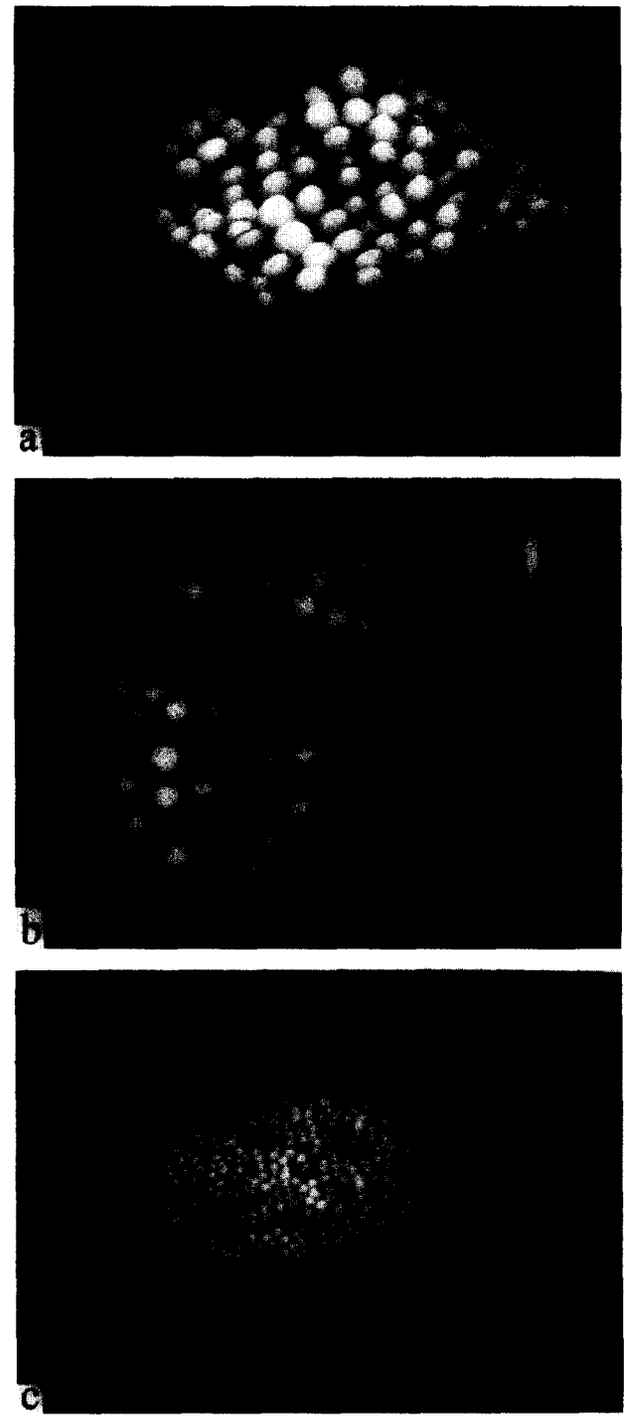

Figure 2 Atomic force microscopy images of films prepared from pure hard latex, $\phi_s = 0$: (a) 1 μm × 1 μm, 3D plot; (b) 1 μm × 1 μm, top view; (c) 2.5 μm × 2.5 μm, 3D plot

but here the added difficulty of particle coalescence makes it even harder to determine an accurate size for the particles in the film[12].

Previous AFM studies of poly(buytl methacrylate) (PBMA) films, prepared from surfactant-free dispersions, show a similar particle arrangement at the film surface, consistent with face-centered cubic (fcc) packing[6,12]. The particles have a truncated spherical shape. As the films are annealed at elevated temperatures, the particles become more flattened, and the peak-to-valley distance diminishes as the annealing is continued. Freeze-fracture transmission electron microscopy studies confirm the presence of fcc order in the interior of these films and demonstrate that the particles in the interior have been deformed into space-filling dodecahedra[13,14]. Small angle neutron scattering measurements reported by Chevalier *et al.*[15] on film formation from poly(styrene-*co*-buytl acrylate) latex dispersions show extensive fcc ordering, and their TEM micrographs are consistent with particle deformation to an ordered array of rhombic dodecahedra.

Figures 4–7 show AFM images, at high and low resolution for each of four different latex blend compositions. The extent of soft particle coalescence is remarkable. An interesting observation common to all blend images is the virtually complete deformation of the soft particles. It seems that as the soft particles deform amongst the hard ones, they simply melt into the interstitial spaces and lose any particulate structure. In fact, the surfaces of the blends with high soft-particle concentrations appear smooth and continuous, indicating that the soft particles have probably coalesced over the entire surface.

At a soft particle volume fraction of 0.2, the hard particles are still apparent as undeformed spheres. However, one can detect a marked difference between this sample and the sample of pure hard latex. In the presence of 20% soft particles, the hard particles seem to be held together by a 'glue' of deformed soft particles. This is especially evident in *Figure 4* (top), where a region

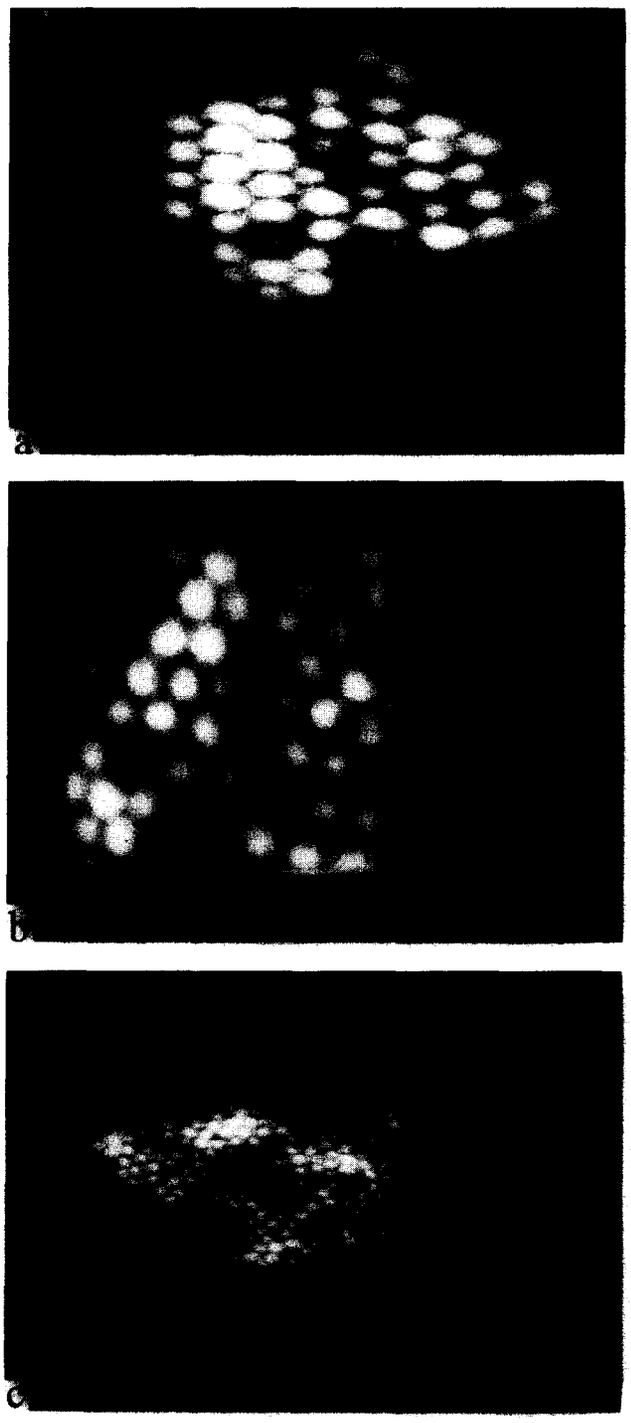

Figure 3 Atomic force microscopy images of films prepared from pure soft latex, $\phi_s = 1.0$: (a) 1 μm × 1 μm, 3D plot, (b) 1 μm × 1 μm, top view, (c) 2.5 μm × 2.5 μm, 3D plot

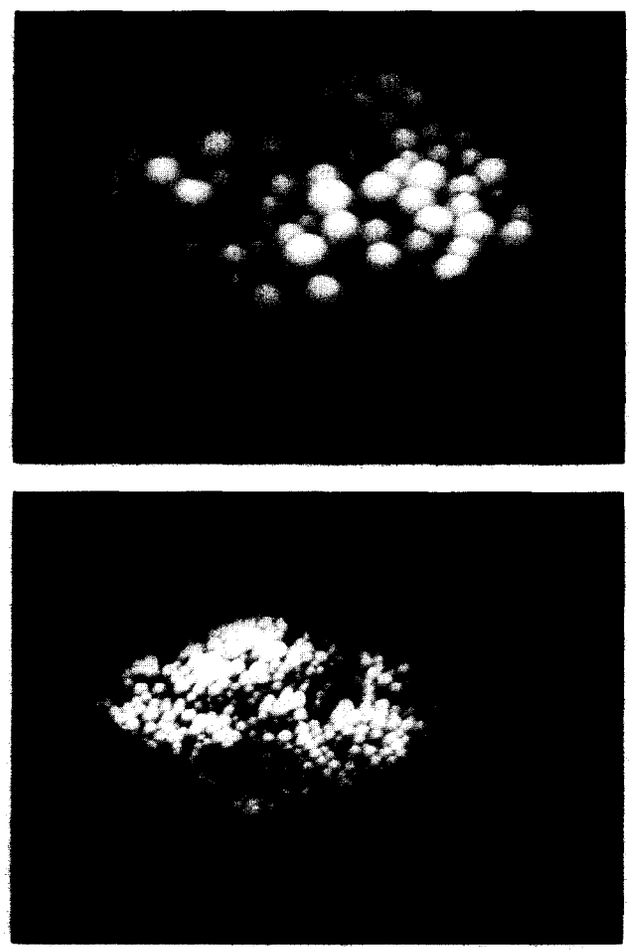

Figure 4 Atomic force microscopy 3D images of films prepared from blends of soft and hard latex, for $\phi_s = 0.2$. Upper, 1 μm × 1 μm plot; lower, 25 μm × 25 μm plot

of deformed soft latex can clearly be seen between the hard particles near the left corner.

In the images where $\phi_s = 0.4$ (*Figure 5*) and $\phi_s = 0.6$ (*Figure 6*), further soft particle coalescence is visible. The most striking change in these images is the presence of bumps which are larger than the size of either of the individual hard or soft particles. This is an indication of particle clustering. Because the bumps are quite smooth and resemble boulders more than spheres, it is reasonable to suppose that the soft particles have deformed and coalesced over the entire surface. Between bumps, one can sometimes see a well-defined boundary which probably corresponds to the juxtaposition of two deformed soft particles. We believe that the bumps arise from the presence of underlying hard particles. This idea is supported by the observation that as the hard particle volume fraction is decreased, the number of bumps also decreases.

The reduction of bumps is most pronounced in the $\phi_s = 0.8$ film (*Figure 7*) where the hard particle fraction is low. Here, the bumps are randomly distributed over the surface of the film within what seems to be a bed of soft particles. If one looks carefully, individual soft deformed particles can be seen within flat regions of the film. The scarcity of hard particles in this film leads to isolated bumps which are easier to analyse than crowded, adjoining bumps. They appear much like truncated spheres, but cannot simply represent a single particle protruding from the bed, because if one were to extrapolate the diameter of the sphere from the observable portion, one would find it to be much larger than that of a single particle. The bumps, therefore, must be produced by soft particles deforming over hard ones.

It is difficult to relate the AFM surface images directly and precisely to the phase diagram data, but general trends are nonetheless evident. As noted, the film turbidity is indicative of the presence of microscopic voids. Therefore, while voids are not apparent at the surface of the film, the amount of space-filling latex at the surface can be taken as an approximate representation of the extent of continuity in the interior. In the $\phi_s = 0.2$

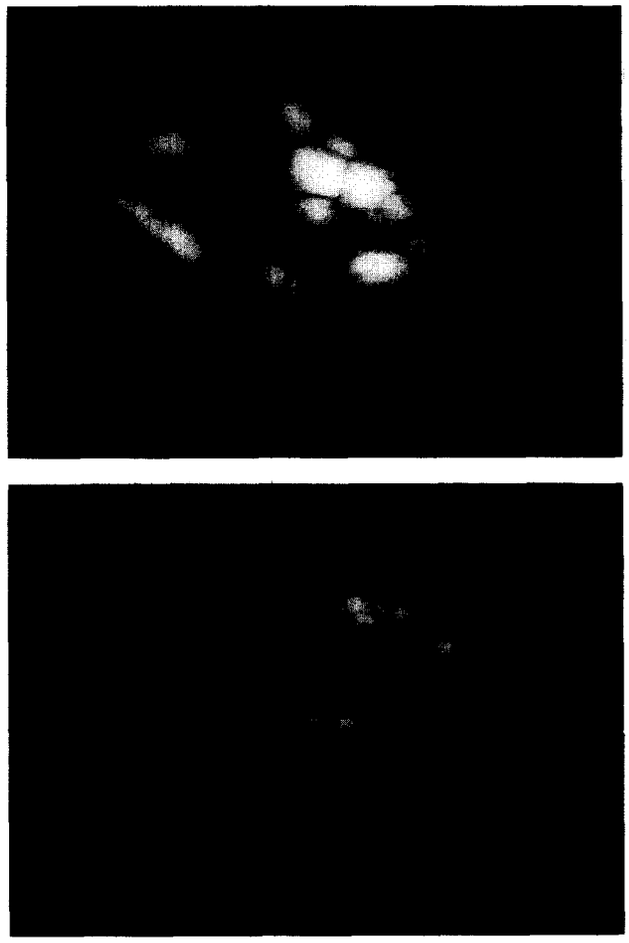

Figure 5 Atomic force microscopy 3D images of films prepared from blends of soft and hard latex, for $\phi_s = 0.4$. Upper, 1 μm × 1 μm plot; lower, 2.5 μm × 2.5 μm

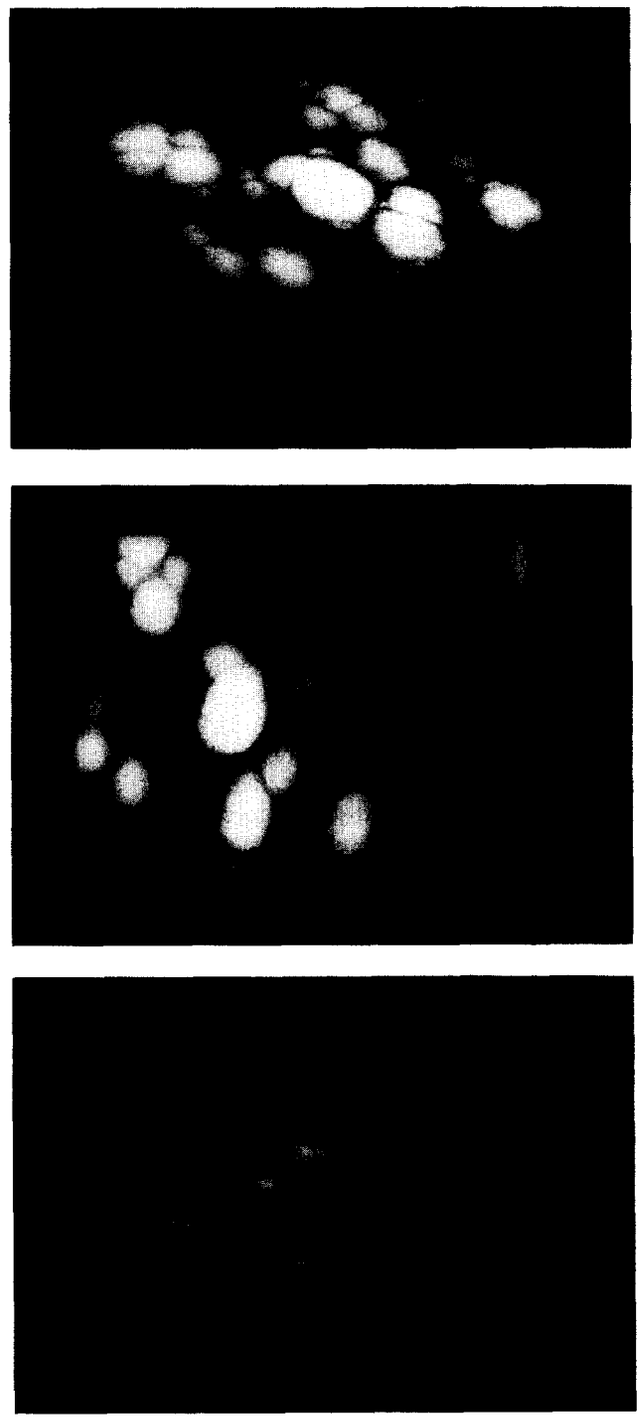

Figure 6 Atomic force microscopy images of films prepared from blends of soft and hard latex, for $\phi_s = 0.6$. Upper, 1 μm × 1 μm, 3D plot; middle, 1 μm × 1 μm, top view; lower, 2.5 μm × 2.5 μm, 3D plot

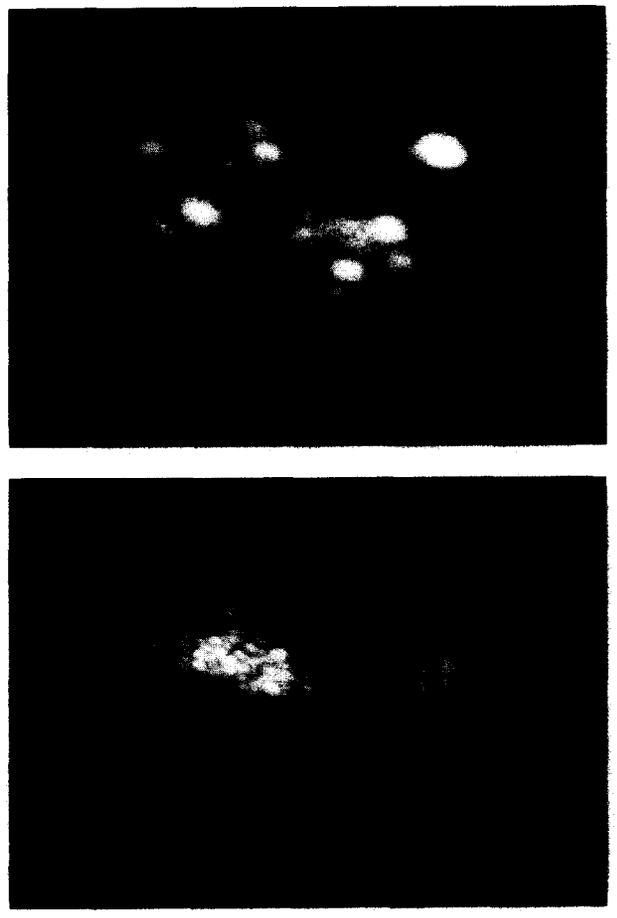

Figure 7 Atomic force microscopy 3D images of films prepared from blends of soft and hard latex, for $\phi_s = 0.8$. Upper, 1 μm × 1 μm, 3D plot; lower, 2.5 μm × 2.5 μm, 3D plot

film, the spaces between hard particles are easily visible, suggesting the presence of extensive voids within. Although the phase diagram shows a transition to void-free films at ϕ_s values greater than 0.5, it is difficult to discern an obvious transition between the AFM images of the $\phi_s = 0.4$ and $\phi_s = 0.6$ films. It is easy to see in the $\phi_s = 0.8$ film that no voids ought to be present, since the hard particles are rarely even adjacent to each other.

Finally, the apparent 'wetting' of the hard particle surfaces in the blend films deserves some comment. The extensive flow of the soft particles at a temperature so close to the T_g of the dry polymer (23°C *versus* $T_g = 17$°C) raises the question of whether forces associated with the lower surface energy of the latex polymer richer in BA provide an additional driving force for plastic deformation. Given the similar composition of the two polymers, the surface energy differences are likely to be small. Plasticization by water may lower T_g and the modulus of the soft polymer significantly. What seems undeniable is that, in the blends, the hard particles become buried under a coating of polymer derived from the soft polymer.

CONCLUSION

In summary, transparent films can be formed from latex blend dispersions consisting of hard and soft particles when the soft particle volume fraction exceeds ≈0.5. By the atomic force microscope technique in the TappingMode™, we obtained basic features of the particular arrangement at the film surface for films of different particle compositions. In general, the hard particles preserve their original size and spherical shape, while the soft particles coalesce into a void-free phase. In blend films when $\phi_s > 0.5$, hard particles are not visible at the surface. Rather, individual hard particles or small clusters of hard particles seem to be coated by deformed soft particles, forming large boulder-like bumps which themselves have a smooth surface. There is no obvious transition in the surface structure of the films of $\phi_s = 0.4$ compared to those of $\phi_s = 0.6$, as seen in the AFM images, yet these films span the transition from significant turbidity to full clarity in the films. This suggests that turbidity arises from voids present in the film interior.

ACKNOWLEDGEMENTS

Funding for this project was provided by the Institute for Chemical Science and Technology and by NSERC, Canada. The authors would like to thank M. Neag and Dr C.-Y. Kuo for analysis of the latex.

REFERENCES

1 Patton, T. L. 'Paint Flow and Pigment Dispersion', Wiley-Interscience, New York, 1979
2 Karsa, D. R. 'Additives for Water-based Coatings', Royal Chemical Society, London, 1990
3 Winnik, M. A., Wang, Y. and Haley, F. *J. Coatings Technol.* 1992, **64(811)**, 51
4 Feng, J., Winnik, M. A., Shivers, R. and Clubb, B. *Macromolecules* 1995, **28**, 7671
5 Friel, J. European Patent Application 0 466 409 A1, 1992
6 Wang, Y., Juhué, D., Winnik, M. A., Leung, O. M. and Goh, M. C. *Langmuir* 1992, **8**, 760
7 Binnig, G., Quate, C. F. and Gerber, Ch. *Phys. Rev. Lett.* 1986, **56**, 930
8 Burnham, N. A. and Colton, R. J. *J. Vac. Sci. Technol.* 1989, **A7**, 2906
9 Winnik, M. A. and Feng, J. *J. Coatings Technol.* **68(852)**, 39
10 Sosnowski, S., Li, L., Winnik, M. A., Clubb, B. and Shivers, R. S. *J. Polym. Sci. Part B: Polym. Phys.* 1994, **32**, 2499
11 Markiewicz, P. and Goh, M. C. *Langmuir* 1994, **10**, 5
12 Goh, M. P., Juhué, D., Leung, O. M., Wang, Y. and Winnik, M. A. *Langmuir* 1993, **9**, 1319
13 Wang, Y., Kats, A., Juhué, D., Winnik, M. A., Shivers, R. S. and Dinsdale, C. J., *Langmuir* 1992, **8**, 1435
14 Roulstone, B. J., Wilkenson, M. C., Hearn, J. and Wilson, A. J. *Polym. Int.* 1991, **24**, 87
15 Chevalier, Y., Pichot, C., Graillat, C., Joanicot, M., Wong, K., Lindner, P. and Cabane, B. *Colloid Polym. Sci.* 1992, **270**, 806